

RESEARCH

Open Access



Experimental and Numerical Evaluation for Hybrid Reinforced T-Beam with Different Ratios of Recycled Rubberized Concrete

Tarik S. El-Salakawy^{1*} , Amr A. Gamal¹ and Mohamed Essam Sayed¹

Abstract

The use of hybrid GFRP and steel bars as main reinforcement increases the flexural capacity of T-section concrete beams and reduces ductility. Adding recycled rubber to the concrete mix would further enhance the ductility of the hybrid system. Evaluation of the concrete's flexural capacity and ductility is the main goal of the current investigation using normal concrete (NC) and rubberized recycled concrete (RRC). Eight T-beams have been experimentally investigated in this research, two beams were reinforced with steel bars and GFRP bars with zero percentage of crumb rubber (C.R). The remaining beams were reinforced with different combinations of GFRP and steel bars with rubberized concrete mixes with partial substitution of sand with recycled crumb rubber by (0%, 7.5%, 10%, and 12.5% replacements by volume) particle size 1.0 to 2.0 mm. The ductility index for the tested hybrid rubberized T-beams (HRTB) BRH1, BRH3a, BRH5, BRH2, BRH4, and BRH6, were higher than BH1 and BH2 by 28.2%, 35.47%, 65.38%, 23.76%, 30.04%, and 56.95% indicating that increasing the percentage of C.R. has a direct effect on increasing the ductility index. The ultimate failure load for the tested HRTB BRH1, BRH3a, and BRH5, decreased by 11.68%, 14.29%, and 17.47% compared to the hybrid T-beam BH1. The energy dissipation decreased for HRTB BRH1, BRH3a, BRH5, BRH2, BRH4 and BRH6 by 7.88%, 12.36%, 17.17%, 8.12%, 12.96%, and 18.28 compared to hybrid T-beams BH1 and BH2. This indicates that the existence of the very weak C.R. was not able to dissipate the energy properly within the concrete matrix. Good agreement was found between the numerical model and experimental results in terms of crack pattern, ultimate loads and deflections.

Keywords Hybrid reinforcement, GFRP bars, RRC (recycled rubberized concrete), T-beams

1 Introduction

Reinforced concrete T-beams with steel bars, when compared to RC members reinforced with GFRP bars perform differently. Once cracking starts, the lower elastic modulus of FRP causes a significant decrease in the flexural stiffness of RC elements reinforced with FRP bars, leading to severe deformations under service

loading circumstances. As a result, the design of RC components reinforced with FRP bars was significantly influenced by the serviceability limit condition. Tensile rupture of GFRP bars, which can occur at the applied point stress or in the mid-span area, is the main cause of flexural failure. The aim of this study was to combine the benefits of FRP bars regarding high strength and reduced cost with steel reinforcement regarding ductility and further enhancement of ductility was introduced using C.R. A significant diagonal crack inside the beam shear span is what causes the shear failure. The horizontal extension of this diagonal crack at the level of the GFRP bars indicated bond failure. The findings showed that the surrounding concrete and FRP reinforcing bars have a

Journal information: ISSN 1976-0485 / eISSN 2234-1315.

*Correspondence:

Tarik S. El-Salakawy
tarek.abdelgalil@feng.bu.edu.eg

¹ Faculty of Engineering at Shoubra, Benha University, Cairo, Egypt



© The Author(s) 2024. **Open Access** This article is licensed under a Creative Commons Attribution 4.0 International License, which permits use, sharing, adaptation, distribution and reproduction in any medium or format, as long as you give appropriate credit to the original author(s) and the source, provide a link to the Creative Commons licence, and indicate if changes were made. The images or other third party material in this article are included in the article's Creative Commons licence, unless indicated otherwise in a credit line to the material. If material is not included in the article's Creative Commons licence and your intended use is not permitted by statutory regulation or exceeds the permitted use, you will need to obtain permission directly from the copyright holder. To view a copy of this licence, visit <http://creativecommons.org/licenses/by/4.0/>.

flawless connection. In addition, they demonstrate how simple it is to modify the ACI Code formulas for modeling deflection response, cracking-ultimate moments, and cracked-effective moments of inertia to simulate the flexural behavior of concrete beams reinforced with FRP reinforcing bars. The tension-stiffening component in Branson's original expression needed to be reduced to practical levels, which required the rational construction of suitable modification variables. With the proper modification factor, computed deflections using this method produce reasonable results that contrast favorably with a more comprehensive unified approach that includes a plausible tension-stiffening model. This approach is limited to rectangular sections and underestimates the deflection of aramid FRP-reinforced beams. The use of a straightforward modification factor that functions effectively for all varieties of FRP bar and beam cross-sectional shapes is suggested. In contrast to other analytical equations, the approach accurately predicts the load–deflection and the moment–curvature response, according to comparisons with experiments. For a variety of geometric and material features, as well as varied loading circumstances, parametric studies are carried out to examine the agreement of the various empirical equations with that of the present approach. (Ashour, 2006; Benmokrane et al., 2021; Bischoff, 2007; Kara & Ashour, 2012; Rasheed et al., 2004). The behavior of RC components reinforced with FRP bars should be better understood to use FRP reinforcement. Numerous studies have concentrated on RC beams using various types of FRP bars. ACI 440.1R-01 can be used. The deflections and fracture widths of six entire concrete beams reinforced with different GFRP reinforcement ratios were measured and compared to those predicted by the proposed models. The experimental findings were consistent with what the model predicted. (Razaqpur et al., 2000; Toutanji & Deng, 2003; Toutanji & Saafi, 2000; Vijay & Gangarao, 2001; Yost & Gross, 2002). The reuse of old tires in various civil engineering projects can have a positive on the environment. Several research studies Concentrated on the use of C.R. particles as a replacement for sand and aggregates at various ratios. (Oikonomou & Mavridou, 2009; Ozbay et al., 2010) The results revealed that as the % of rubber replacement increased in the concrete mix, the mechanical characteristics of concrete decreased and its workability decreased. (Najim & Hall, 2010, 2012; Zheng et al., 2008) The findings demonstrated that raising the C.R. seems to decrease the weight of concrete, decrease crack width and improve deformability under a given force. On the other hand, initial crack and ultimate flexural were significantly decreased when a high percentage of C.R. (above 15%) was used. (Ismail &

Hassan, 2017; Mendis et al., 2018). According to test results, adding more rubber reduces the concrete's compressive strength and elastic modulus. Concrete mixes that are suitable for safety barriers made of concrete in places where strength, fracture toughness, and energy dissipation are required can be made by substituting up to 20–40% of the aggregates with crumb rubber. (Atahan & Yücel, 2012; Liu et al., 2012; Sukontasukkul et al., 2013) The critical crack mouth opening displacement (CMOD_{cri}) was also noticeably elevated by thermal damage resulting from heating from 25 to 600 °C (Guo et al., 2014). The findings show that when compared to regular NC concrete, reinforced recycled aggregate concrete RRAC with an appropriate rubber content exhibits good compressive behavior. Reinforced recycled aggregate concrete is also a more environmentally friendly alternative to normal rubber concrete for use in the flexural members of concrete structures (Xie et al., 2015). Load–displacement behavior was analyzed for the plain and hybrid concrete beams under static and impact loads were considered in previous studies. The results showed that most of the time hybrid beams were utilized, several characteristics improved, including stress, modulus of rupture, stiffness, failure pattern, and ultimate load. The strain capability of the RRC beams was raised (Ahmed, 2017; Alasmari et al., 2019; Al-Tayeb et al., 2012). The ultimate flexural loads and behavior of concrete slabs reinforced with BFRP were better than those of concrete slabs reinforced with steel reinforcement, according to the experimental test findings. In addition, the theoretical development of finite element models using the software ANSYS 2019-R1 was used to validate the structural behavior of the tested slabs, and in first cracking loads, load-carrying capacity, fracture pattern, and deflection. The effect of the hybrid reinforcement ratio on the flexural performance of concrete beams in both under and over-reinforced scenarios was examined using three-dimensional finite element models. When comparing standard steel-reinforced concrete with fiber-reinforced polymer (FRPRC), the former displays a more ductile behavior. The flexural performance of hybrid FRPRC is significantly influenced by the ratio, or A_f/A_s , of hybrid reinforcement between steel and FRP (Erfan et al., 2021; Qin et al., 2017). The flexural performance of engineered cementitious composite (ECC) concrete beams reinforced with innovative hybrid bars was conducted using FRP or steel bars, proving that hybrid bars improved ultimate strength and ductility. According to the test results, ECC concrete beams reinforced with hybrid bars or hybrid schemes had significantly increased carrying loading capacity. The achieved enhancements are 12% and 27% for polyvinyl alcohol (PVA) ratio of

0.75% and 1.5%, respectively (Said et al., 2020). The results indicated that both the fracture toughness and fracture energy increased with the increase of the rubber content (Guo et al., 2014). A reduced number of wastes of recycled origin may be used in structural OPC concretes (Miraldo et al., 2021). Crumb rubber was substituted in multiples of 2.5% from 0 to 20%. These concrete samples underwent tests to ascertain the depth of carbonation, water absorption, compressive strength, weight change, and chloride penetration of these specimens under acid attack. It is clear from the test findings that high-strength rubberized concrete is extremely resistant to harsh situations (Thomas et al., 2015). By substituting micro-scale C.R. for sand, experiments have been conducted to preserve the electrical resistivity, damping qualities, Compressive, tensile, and flexural strengths of RRC with high strength. The findings of static and dynamic tests showed that certain recycled sign posts might make good substitutes for traditional wooden posts. The compressive strength of reinforced self-consolidating rubberized concrete (SSCRC) mixtures was adversely influenced by increasing the proportion of C.R. (AbdelAleem et al., 2018; Atahan & Yucel, 2013; Kaewunruen et al., 2018; Onuaguluchi & Panesar, 2014). It was discovered that, in comparison to regular concrete, RRC is less ductile, more resilient to cracks, and has a lower compressive strength (Alam et al., 2015). When fine aggregates are replaced with C.R. to the extent of 5% and 10%, reinforced concrete beam performance is demonstrated to be satisfactory. Both the toughness and performance of rubber concrete with steel fibers increased as the proportion of rubber exceeded 10% (Eisa et al., 2020). Finite element analysis and concrete damage plasticity models are used to perform three-dimensional non-linear numerical simulations and parametric evaluations. The parametric study's findings allowed for a quantitative assessment of the degree of confinement offered by the transverse reinforcement as

well as a direct evaluation of the inelastic behavior in terms of strength and deformation qualities. (Xu et al., 2020). Because GFRP is brittle, beams lose some of their flexibility. HRRC reinforcement has been suggested as a way to increase beam ductility while maintaining the high strength characteristic of GFRP bars. The ratio of GFRP to steel bars in the mid-span section and the effect of C.R. on the HRRC matrix were the main study parameters.

2 Experimental Program

The performance of hybrid reinforced T-beam with recycled rubberized concrete was investigated in this investigation, which was conducted at the Housing and Building National Research Centre in Dokki, Egypt. Estimating the ultimate loads, deflections, cracks, mode of failure, and ductility index for the tested beams was the aim of the study.

2.1 Specimens

The performance of eight concrete beam specimens containing hybrid reinforced concrete beams was investigated as listed in Table 1 and Fig. 1. The beams were simply supported and subjected to a two-point loading test and the schematic diagram for the eight beams and reinforcement along with the C.R value are represented in Fig. 2.

3 Materials

A control mix of normal concrete NC with a target compressive strength of 40 MPa and another mix for rubberized concrete with 35 MPa was used in developing rubberized concrete mixtures. A concrete mix of ordinary Portland cement with a relative density of 3.15 gm/cm³, a 0.43 ratio of water to cement, potable water, natural crushed stone coarse aggregates with a relative density of 2.57 g/cm³ and a maximum size of 10 and 20 mm. And fine aggregates with a relative density of 2.60 gm/cm³. A

Table 1 Beams reinforcement and studied parameters

Model	Bottom reinforcement	Top reinforcement	Bottom reinforcement	A _f /A _s (bot.)	% (C.R)*
BH1 (Control specimens)	2Ø10F + 2Ø10S	2Ø10	GFRP + Steel	1	0
BH2 (Control specimens)	2Ø12F + 2Ø10S	2Ø10	GFRP + Steel	1.43	0
BRH1	2Ø10F + 2Ø10S	2Ø10	GFRP + Steel	1	7.5
BRH2	2Ø12F + 2Ø10S	2Ø10	GFRP + Steel	1.43	7.5
BRH3a	2Ø10F + 2Ø10S	2Ø10	GFRP + Steel	1	10
BRH4	2Ø12F + 2Ø10S	2Ø10	GFRP + Steel	1.43	10
BRH5	2Ø10F + 2Ø10S	2Ø10	GFRP + Steel	1	12.5
BRH6	2Ø12F + 2Ø10F	2Ø10	GFRP + Steel	1.43	12.5

* Partial substitution (0%, 7.5%, 10%, and 12.5% replacements by volume) of sand by recycled crumb rubber, A_f/A_s (bot.) = area reinforcement of GFRP bars/ area reinforcement of steel bars, 2Ø10S = 2bars diameter 10 mm steel bars, 2Ø12F = 2bars-diameter 10 mm GFRP bars

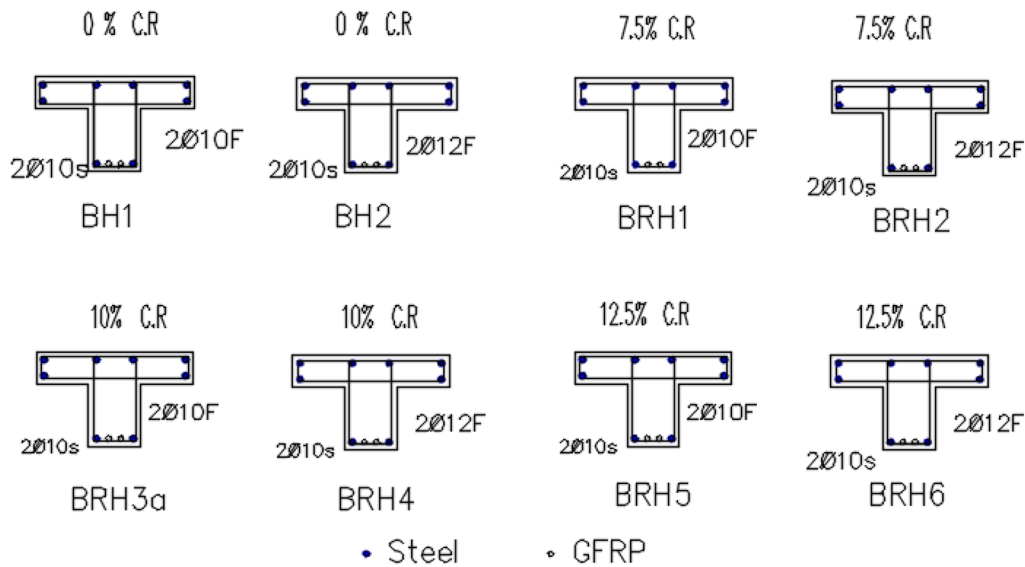


Fig. 1 The tested specimen's reinforcement and dimensions

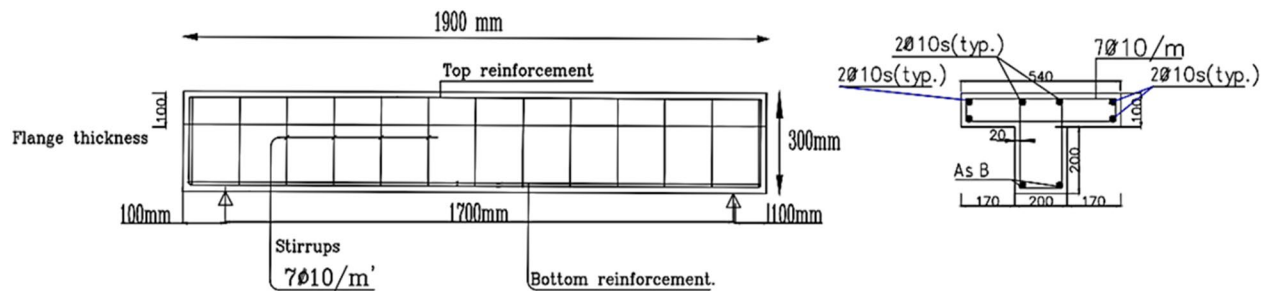


Fig. 2 Schematic longitudinal section of the tested specimen's beam and dimensions

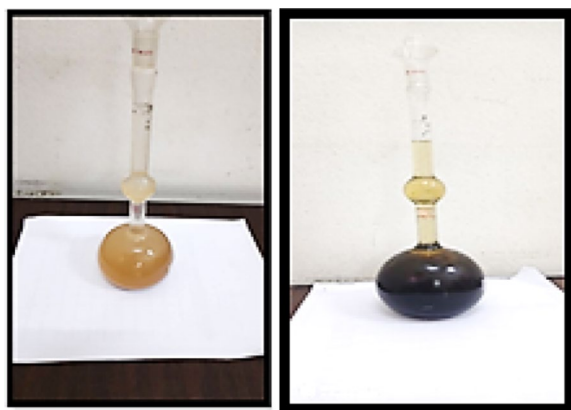


Fig. 3 Specific gravity of fine aggregate and the C.R

maximum size from 1 to 2 mm of crumb rubber with a relative density of $1.14 \pm 0.02 \text{ gm/cm}^3$ is shown in Fig. 3, Fig. 4, respectively. Superplasticizer (SikamentR-2004)

was used with a density of 1200 kg/m^3 (at 20°C ASTM C 494/C494M-19e1) (ASTM, 2020) to reduce water and enhance workability, the mix NC with 0% C.R. and the concrete mix rubberized reinforced concrete (RRC) has the C.R. 7.5%, 10%, and 12.5% as partial replacement of sand by volume are listed in Table 2.

A 1000-kN capacity testing device applied the loads to the specimens as shown in Fig. 5 and Fig. 6. The maximum strain was determined similarly.

GFRP bars used in the experimental with 10mm and 12mm diameters with a tensile strength of (910–989) MPa. The steel rebar had a diameter of 10, and 12 mm with yield stress and tensile strength are 540 and 641 MPa, respectively, listed in Table 3; see Fig. 6. Tensile strength of GFRP bars was about 1.5 times that of reinforcing steel.

Mixing concrete was performed using a concrete tilting drum mixer. The mixing time was about three minutes. The slump test was from 13 to 16 cm which was suitable for pouring reinforced concrete in beams The C.R.

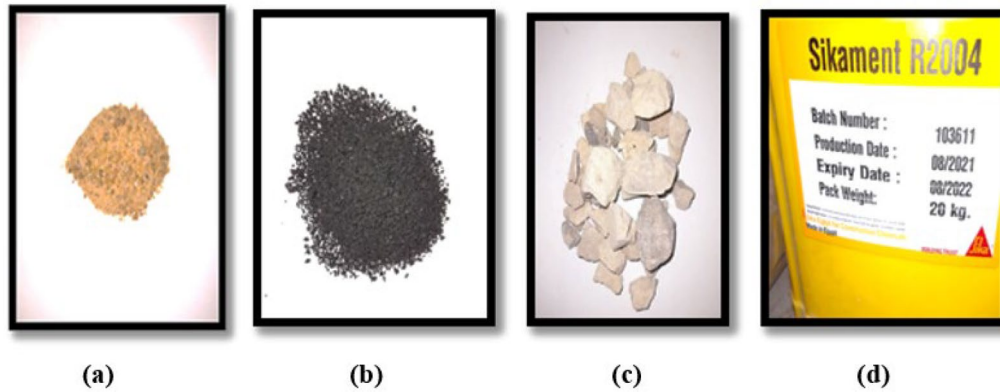


Fig. 4 a Fine aggregate (sand), b recycled fine crumb rubber sample—c size (1–2 mm) coarse aggregate and d HRWR (Sikament R2004)

Table 2 Mix proportions for concrete mixes with 0, 5%, 7.5%, 10%, 12.5, and 15% of sand replacement by recycled crumb rubber per cubic meter (kg/m³)

Mix type	C.R (%) *	Cement	W/C	Water	SP	Fine aggregate (sand)	Coarse aggregate	C.R
		W (kg)		W (kg)	W(kg)	W (kg)	W (kg)	W (kg)
NC (0%C. R)	0	400	0.43	172	5.5	681	1120	0
RRC (5%C. R)	5	400	0.43	172	5.5	646	1120	14.9
RRC (7.5%C. R)	7.5	400	0.43	172	5.5	630	1120	22.4
RRC (10%C. R)	10	400	0.43	172	5.5	612	1120	29.8
RRC (12.5%C. R)	12.5	400	0.43	172	5.5	592	1120	37.3
RRC (15%C. R)	15	400	0.43	172	5.5	579	1120	44.8

* Ex.-Weight of C. R = (7.5/100) (1140/2600) *681

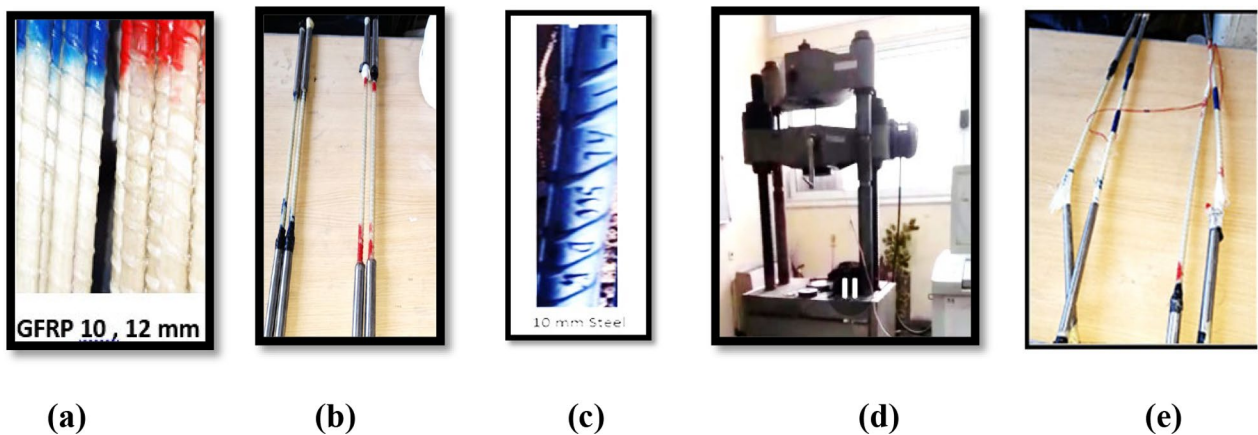


Fig.5 a Samples of GFRP fiber bars, b preparing samples of GFRP, FRP c steel bar, d testing of tensile strength for FRP and steel bars, e specimen after testing

increased the workability of the concrete mix. The forms were constructed from clean wood, and their interior surfaces were coated with oil before casting. The concrete was compacted and physically placed using an internal electrical vibrator as shown in Fig. 7. After a day, the

wood forms were removed, and the 28-day daily curing procedure started. Results for Young’s modulus (E) are shown in Table 4, Fig. 8.

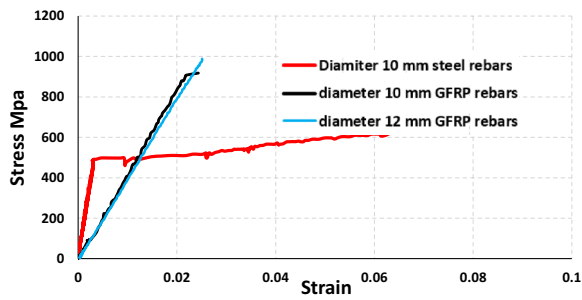


Fig.6 Stress–strain curve for 10mm, 12mm steel and GFRP rebars

a two-point static load. To convert the applied concentrated load into a two-point load on the tested beam, the applied load was transferred from the load cell to a steel I-beam plate, as shown in Fig. 9. A single longitudinal strain gauge was fastened to the specimens’ center. The test machine’s load cell measured the load. Differential transformers (LVDTs) were used to measure the deformation of the beams, where Strain gauges were used for measurement of the strain of GFRP and steel. The system of a data logger was employed to automatically gather the test data, as shown in Figs. 10, 11.

3.1 Test Setup

After 28 days of age, all beams were only supported and put through testing with a 500-ton testing device under

Table 3 Mechanical properties of reinforcement bars

Material	Diameter (mm)	Area (mm)*	Yielding strength(MPa)	Tensile strength(MPa)	Modulus of elasticity(GPa)
GFRP	10	74.7	–	910	40
GFRP	12	87.30	–	989	40
Steel	10	78.5	540	641	200

* Area supplied by the manufacture

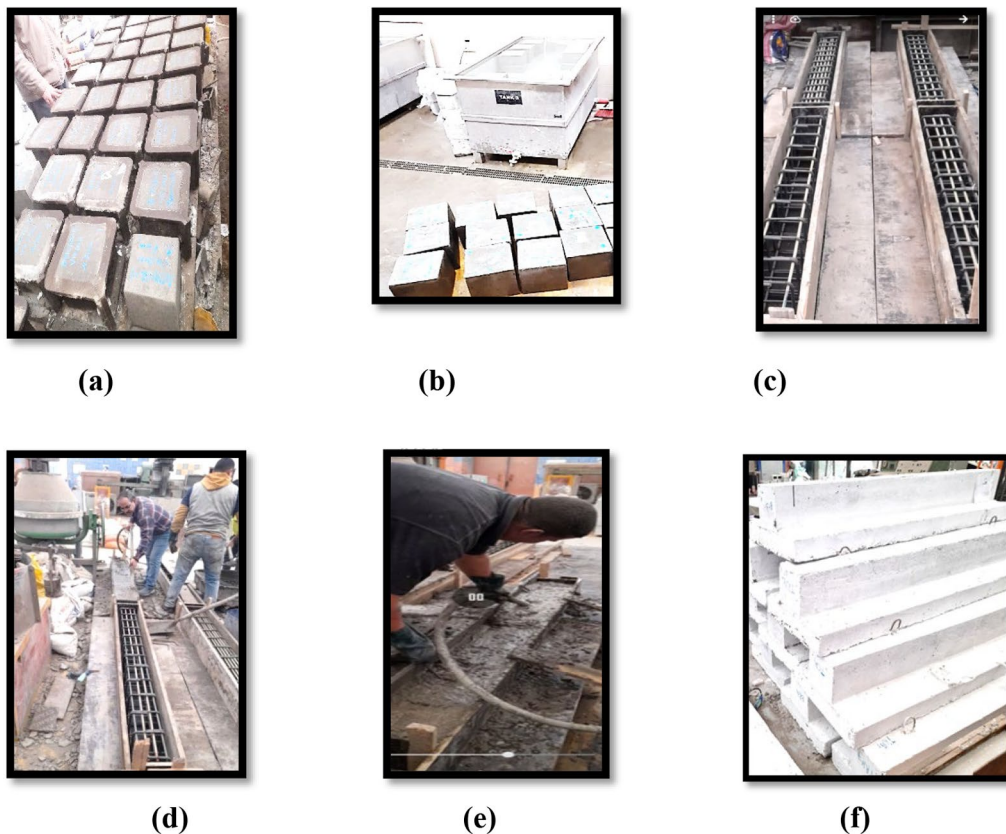


Fig.7 Specimen preparation: **a** preparation of cubes, **b** curing, **c** steel reinforcement, **d** casting the concrete, **e** finishing, **f** all finishing T-section beams

Table 4 Determination of Young’s modulus for the differential type of concrete different concrete mixes

Concrete mixes	Young’s modulus MPa
NC (0%C. R)	32911.95
RRC (7.5%C. R)	23546.76
RRC (10%C. R)	19580.12
RRC (12.5%C. R)	19166.56

4 Experimental Results

In this chapter, the effect of GFRP and steel bars with rubberized concrete mixtures including some substitution of sand with recycled C.R. by (0%, 7.5%, 10%, and 12.5% replacements by volume) were analyzed according to the recorded data. The test results of the specimens are presented.

The average concrete compressive strength was found by testing three cubes for each beam after 7 days and 28 days; see Table 5. The loss in compressive strength was more noticeable when the concrete specimens made with

RRC were mixed with those made with the control mix (Thomas et al., 2015).

Beams BH1, BH2, BRH1, BRH2, BRH3a, BRH4, BRH5 and BRH6 have ultimate loads of 269, 270, 237, 240, 230,234, 222, 227 kN, respectively. The deflection at ultimate load 50, 51, 53, 54, 55, 56, 58, 59 mm is listed in Table 6 (Moolaei et al., 2021). The mode of failure is flexural failure and the crack pattern of failure for the beams is listed in Table 7.

Total load capacities for the tested hybrid rubberized T-beam BRH1, BRH3 and BRH5 (7.5%,10%, and 12.5% C.R) were decreased by 11.89%, 14.49%, and 17.47%, respectively, compared to the hybrid T- beam BH1(0% C.R as shown in Fig. 12.

All beams were visually observed during the flexural test, and first crack have been observed and recorded relative to the corresponding loads, the yielding and ultimate loads, and the failure loads are listed in Table 6 and shown in Fig. 12.

The maximum and minimum deflation recorded 59 59.0mm, and 50.0 mm for BRH6 and BH1, respectively, as shown in Fig. 13. The deflections obtained for all tested

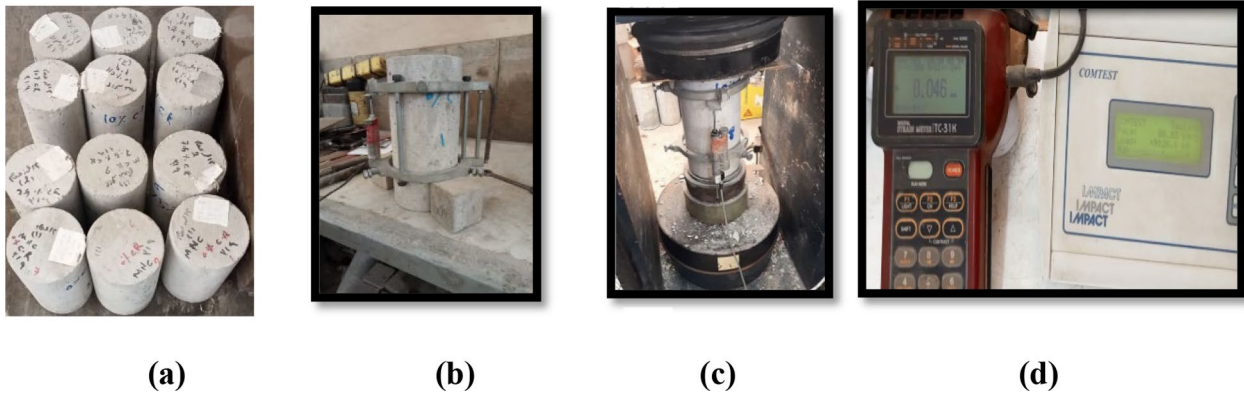


Fig.8 Specimen preparation for determine Young’s modulus. **a** Preparing of cylinders. **b, c** Testing. **d** Measuring the load and strain



Fig.9 The test loading of the specimens, LVDT and strain gages for specimens



Fig.10 Hydraulic jack (5000 K N) on the loading plates

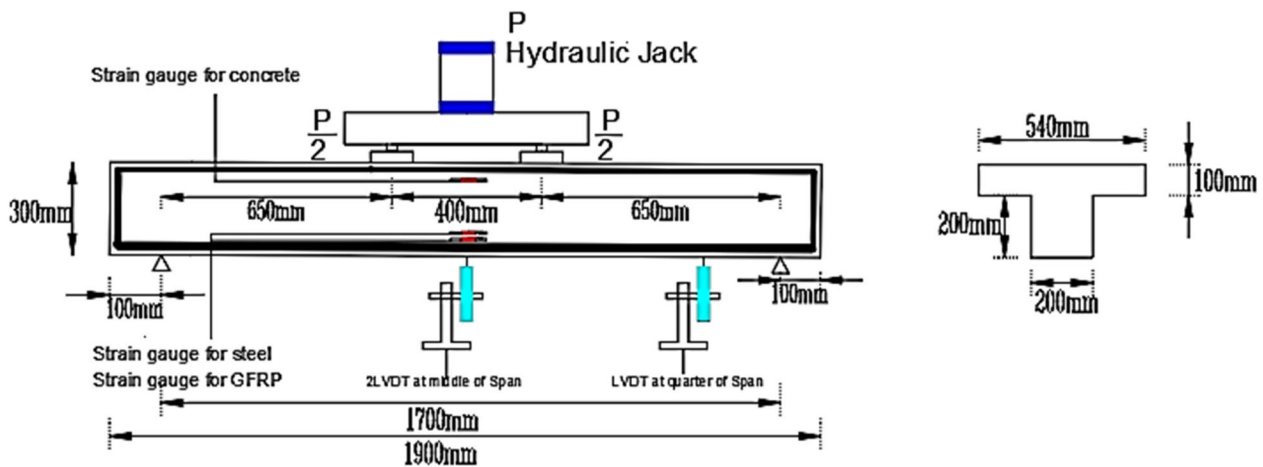


Fig.11 Test setup schematic diagram

Table 5 Compressive strength f_c (MPa) for cubes dimension 150*150mm for the different concrete mixes

Concrete mixes	Average ultimate compressive strength f_{cu} (MPa)		
	7 days	28 days	% Of NC*
NC (0%C. R)	34.70	40.00	100
RRC (7.5%C. R)	29.30	35.00	87.5
RRC (10%C. R)	28.4	32.00	80.0
RRC (12.5%C. R)	23.34	28.8	67.0

* As percentage of concrete compressive strength

beams are indicated in Fig. 14. This shows the effect of increasing the C.R. on increasing the deflection at the same level of reinforcement of the beams BH1 and BH2.

Beams BH1 and BH2 flexural capacity increased compared to the other beams compared with the beams

BRH1, BRH2, BRH3, BRH4, BRH5 and BRH6 due to the effect of increased percentage of C.R. as listed in Table 6.

5 Discussion of Results

The effect of GFRP and steel bars with RRC mixes with partial substitution of sand with recycled C.R. by (0%, 7.5%, 10%, and 12.5%) replacements by volume were analyzed according to the recorded data. The test results of the specimens are presented.

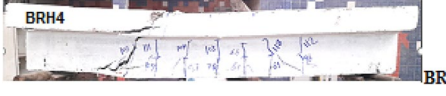
5.1 Ultimate Load Comparisons

The ultimate flexure failure load for the tested hybrid rubberized T-beam BRH1, BRH3a and BRH5 (7.5%, 10%, and 12.5% C.R) decreased by 11.68%, 14.49%, and 17.47%, respectively, compared to the hybrid T-beam BH1(0% C.R) as shown in Fig. 15a. Also the ultimate flexure failure load for the hybrid rubberized T-beam BRH2, BRH4

Table 6 Experimental results at cracking loads, yielding loads and ultimate loads of test specimens

Beam model	Cracking loads		Yielding loads		Ultimate(peak) loads	
	P _{cr} (kN)	Δ _{cr} mm	P _{ie} (kN)	Δ _y mm	P _u (kN)	Δ _u mm
BH1	44	0.69	102	11.22	269	50.0
BH2	48	0.70	104	9.67	270	51.0
BRH1	50	1.01	38	8.65	237	53.0
BRH2	55	1.59	95	12.29	240	54.0
BRH3a	46	0.89	70	5.98	230	55.0
BRH4	45	0.76	108	8.05	234	56.0
BRH5	59	0.96	92	9.61	222	58.0
BRH6	60	1.31	98	10.3	227	59.0

Table 7 Experimental results of cracking load, yield load, ultimate load capacity, and mode of failure

Crack patterns of failure for the beams	Failure mode	Ultimate load L _u (kN)	Yield load L _y (kN)	First crack load P _{cr} (kN)	Beam model
BH1 (Control specimens)	20.80	33.02	87.75	Flexural failure	 BH1
BH2 (Control specimens)	22.02	33.85	87.42	Flexural failure	 BH2
BRH1	16.25	29.37	77.03	Flexural failure	 BRH1
BRH2	17.94	30.99	78.0	Combined of flexural failure + shear failure with debonding*	 BRH2
BRH3a	15.09	22.75	74.75	Combined of shear failure + compression failure	 BRH3
BRH4	18.76	33.85	76.05	Combined of Flexural failure + shear failure with debonding*	 BRH4
BRH5	19.17	30.99	72.15	Combined of flexural + shear failure	 BRH5
BRH6	17.95	31.81	73.77	Combined of flexural failure + shear failure with debonding*	 BRH6

* Debonding mode of reinforcing rebars related to small, developed length, *M_{cr} = cracking moment

and BRH6 (7.5%, 10%, and 12.5% C.R) were lower than the hybrid beam BH2 (0% C.R) by 13%, 15.72%, and 16%, respectively, as shown in Fig. 15b. This indicates that the load-carrying capacity of hybrid rubberized T-beams decreased compared to the reference hybrid T-beams

as shown in Fig. 12 due to decreasing the compressive strength of the rubberized concrete specimens compared to NC specimens (AbdelAleem et al., 2018; Thomas et al., 2015). This was attributed to the effect of increasing the

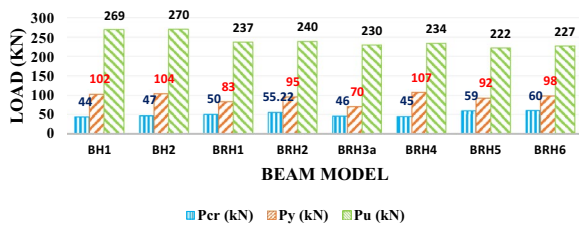


Fig.12 First crack load, yield load and ultimate loads of test specimens

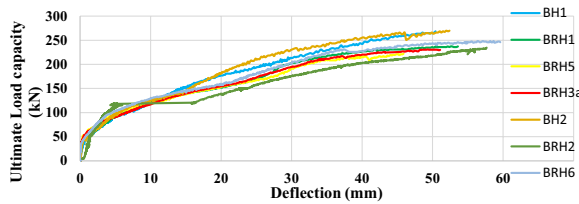


Fig. 13 Experimental load–deflection curve at mid-span

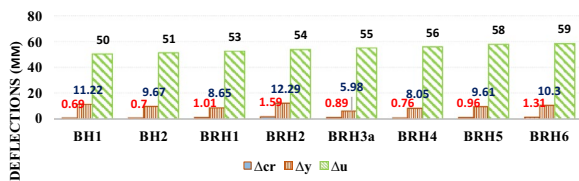


Fig.14 Corresponding deflections for the loads

percentage of crumb rubber in the concrete mix; these results are compatible with the compressive strength results of concrete cubes (AbdelAleem et al., 2018; Thomas et al., 2015) as shown in Table 4. It was noted that increasing the diameter of GFRP bars from 10 to 12mm had minimal effect on the ultimate flexure failure load.

5.2 Deflection Discussions

The maximum deflection at mid-span for the tested hybrid rubberized T-beam BRH1, BRH3a and BRH5 (7.5%,10%, and 12.5% C.R) increased by 4.66%, 9.28%, and 15%, respectively, compared to the hybrid T- beam

BH1(0% C.R) as shown in Fig. 14. Also the maximum deflection at mid-span for the tested hybrid rubberized T-beam BRH2, BRH4 and BRH6 (7.5%, 10%, and 12.5% C.R) increased by 5.26%, 9.16%, and 14.32, respectively, compared to the reference hybrid beam BH2 (0% C.R), as shown in Fig. 14 due to the effect of increasing the percentage of crumb rubber replacement to sand in the concrete mix. Compared to the hybrid beam, the RRC beam has improved the stress–strain curve, and ultimate deflection (Alasmari et al., 2019).

5.3 Ductility Index

The ductility of the structure refers to the deformation capacity from the start of yielding to the maximum bearing capacity or when the load does not significantly decrease after yielding (85% of the peak load) (Sun et al., 2019).

The maximum ductility index recorded was 4.32 for BRH1 mm and the minimum 2.23 mm for BH2 as listed in Table 8, Fig. 16. The ductility indices for the tested rubberized hybrid T-beams BRH1, BRH3a and BRH5 with 10-mm-diameter GFRP bars were higher than the beam BH1 by 28.2%, 35.47%, and 65.38%, respectively as shown in Fig. 17. This indicates that the ductility index of hybrid-rubberized RC T-beams increased with the increase in the percentage of rubber from 7.5% to 10%, and up to 12.5% C.R. The ductility of concrete mixes are increased by an appropriate rubber component (Guo et al., 2014). This trend was observed in GFRP bars 10 mm as shown in Fig. 16.

The ductility indices for the tested rubberized hybrid T-beams BRH2, BRH4 and BRH6 with 12-mm-diameter GFRP bars were higher than the beam BH2 by 23.76%, 30.04%, and 56.95%, respectively, indicating that the ductility index of hybrid-rubberized T-beams with 7.5%, 10%, and 12.5% C.R. showed a continuous increase in ductility index as the percentage of crumb rubber increased (Guo et al., 2014) as shown in Fig. 18. It was also noted that increasing the diameter of GFRP bars from 10 to 12 mm resulted in a decrease in the ductility index in all groups 7.5%, 10%, and 12.5%.

It should also be considered that increasing the diameter of GFRP bars from 10mm in BH1 to 12 mm in BH2

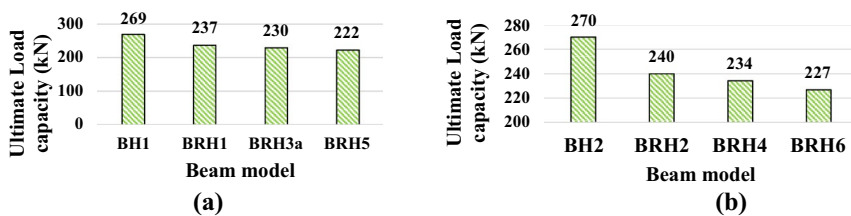


Fig. 15 The load capacity for beams

Table 8 Ductility index for test specimens

Beam model	Ductility $\mu u = \Delta u / \Delta y$ ductility index
BH1	2.34
BH2	2.23
BRH1	3.00
BRH2	2.76
BRH3a	3.17
BRH4	2.90
BRH5	3.87
BRH6	3.50

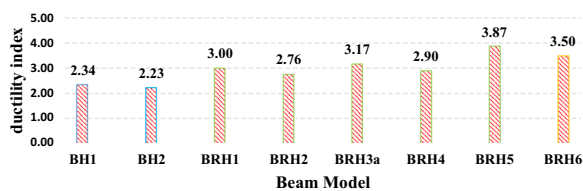


Fig. 16 Specimen ductility index

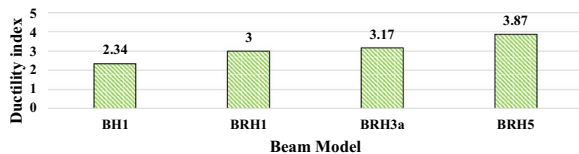


Fig. 17 Ductility index for the beams BH1, BRH1, BRH3 and BRH5

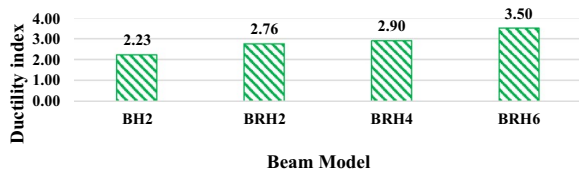


Fig. 18 Ductility index for the beams BH2, BRH2, BRH4 and BRH6

resulted in a decrease in the ductility index by 4.7%, yet the existence of C.R in BRH1 compared to BH1 resulted in regaining an increase in the ductility index by 28%. In terms of the stress–strain curve, ultimate deflection, ductility index, and strain as measured by the two gauges (steel bar and concrete), the rubberized beam performs better than the hybrid beam (Alasmari et al., 2019; Guo et al., 2014).

5.4 Energy Dissipation

The energy absorption of beams is a good criterion for calculating the energy dissipation of models. Based on the region beneath their load–displacement diagrams,

Table 9 Experimental results of the energy dissipation for test specimens

Beam model	Energy dissipation (Ed) Ed(kN.mm)
BH1	10015
BH2	10340
BRH1	9225
BRH2	9500
BRH3a	8750
BRH4	9000
BRH5	8295
BRH6	8450

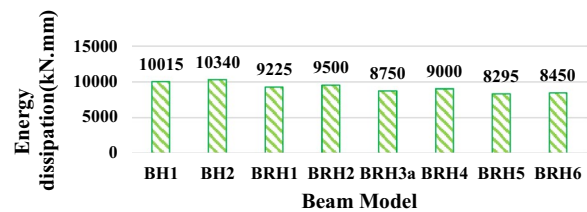


Fig. 19 Tested beam’s energy dissipation

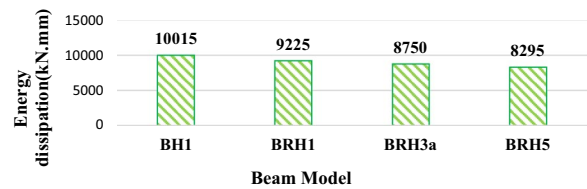


Fig. 20 The energy dissipation for the T-beam BH1, BRH1, BRH3a and BRH5

the samples’ energy absorption is measured up to 85% of the fiber-reinforced beams’ ultimate strength (Moolaei et al., 2021). The energy dissipation of all samples has been computed as listed in Table 9. The lowest energy dissipation was recorded in sample BRH6. The highest energy dissipation for hybrid samples was BH2, meanwhile, the highest energy dissipation for hybrid-rubberized samples was BRH2; see Fig. 19. Also increased effective A_f / A_s (bot.) ratios were associated with increased observed energy absorption in hybrid beams (Moolaei et al., 2021).

Energy dissipation decreased for hybrid-rubberized T-beams BRH1, BRH3a and BRH5 (7.5%, 10%, 12.5% C. R) by 7.88%, 12.36%, and 17.17%, respectively, compared to RC T-beam BH1 (0% C.R.); see Fig. 19. Energy dissipation decreased for hybrid-rubberized T-beams

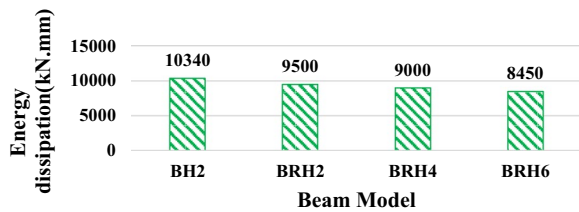


Fig.21 The energy dissipation for the T-beam BH2, BRH2, BRH4 and BRH6

BRH1, BRH3a and BRH5 (7.5%, 10%, 12.5% C.R) by 7.88%, 12.36%, and 17.17%, respectively, compared to RC T-beam BH1 (0% C.R); see Fig. 20.

The energy dissipation decreased for hybrid-rubberized T-beams BRH2, BRH4 and BRH6 with (7.5%, 10%, and 12.5% C.R) by 8.12%, 12.96%, and 18.28% times, respectively, compared to RC T-beam BH2 (0% C.R); see Fig. 21. This indicates that the existence of the very weak crumb rubber was not able to dissipate the energy properly within the concrete matrix, which is an indication of slight lack of compatibility.

6 Methodology and Numerical Model

Given the multitude of elements influencing the flexural behavior of hybrid rubberized concrete HRC reinforced with a combination of steel and glass fiber-reinforced polymer (GFRP) bars, a comprehensive parametric analysis was performed using the finite element analysis program (ANSYS 15). The finite element model's results demonstrate that by carefully designing the hybrid reinforcement ratio, it is possible to achieve the required strength and ductility performance. (Qin et al., 2017). This research looked at the inelastic behavior of rubberized concrete reinforced using a hybrid of T-beams and glass fiber-reinforced polymer (GFRP) bars and steel. Finite element analysis was used to perform parametric evaluations and extensive three-dimensional non-linear numerical simulations. Additionally, it includes all the necessary instructions for building the hybrid rubberized concrete HRC and reinforced concrete models that were needed to analyze the flexural behavior and deflection. The analysis describes the failure modes, central deflection and ultimate load load-carrying of the beams. ANSYS version 15 was used to create a numerical model that was used to validate the results of the eight tested beams. Solid 65 components, which have non-linear properties and can crush in compression and fracture in tension, were used to model concrete. Eight nodes, each with three degrees of freedom, define the element (SAS IP, 1999). A typical element is shown in both local and global Cartesian coordinates in Fig. 22. It is defined in ANSYS by the linear behavior of concrete material with a

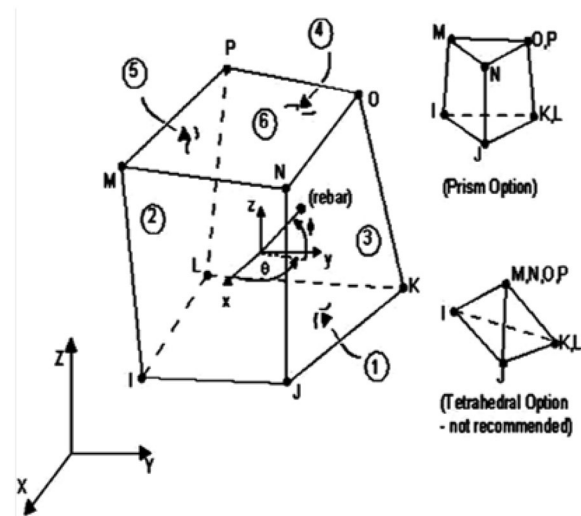


Fig.22 Solid 65 element (SAS IP, 1999)

poison's ratio of 0.2 and the modulus of elasticity derived from experimental tests by various concrete types and mixes. Furthermore, an open shear coefficient of 0.3 and a closed shear coefficient of 0.8 were used to characterize the non-linear behavior (SAS IP, 1999). The actual values of compressive strength f_{cu} were obtained from the experimental program.

The link180 element was used to model GFRP and steel rebars. With two nodes possessing three degrees of freedom, the element is a biaxial compression-tensile element. As seen in Fig. 23, it also featured plasticity, stress stiffness, and deflection.

The elasticity modulus of 200,000 MPa and a Poisson's ratio of 0.3 were the linear assumptions made for the material definitions of the steel element. Through experimental testing, the yield stress for flexural reinforcement was determined to be 540 MPa. The GFRP element's material definitions were predicated on a linear elasticity modulus of 40,000 MPa and a poison's ratio of 0.3. For the GFRP rebar, the yield stress was determined to be 910 MPa through experimental testing. Solid 45 elements were used to model the load

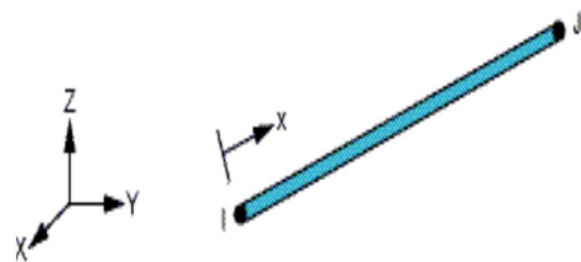


Fig. 23 Discrete element link 180 (SAS IP, 1999)

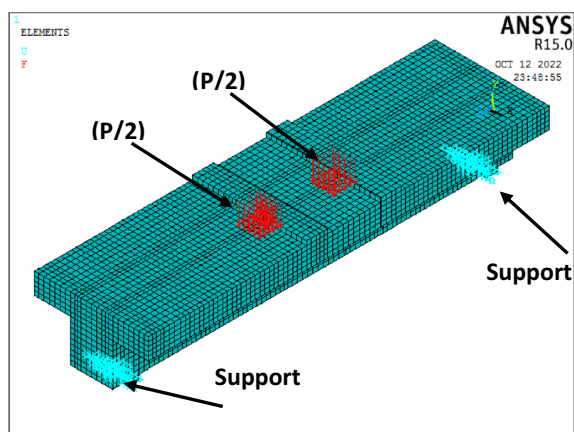


Fig. 24 Boundary conditions and loads applied to beams

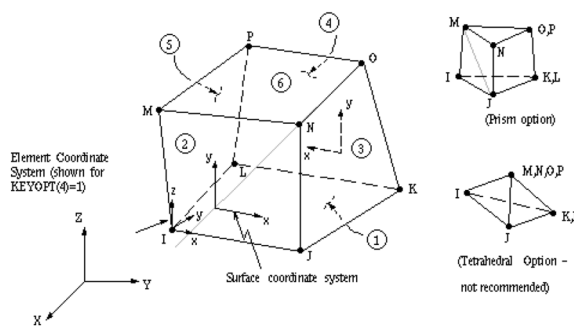


Fig. 25 Solid 45 element in ANSYS (SAS IP, 1999)

plate and supports. Eight nodes with three degrees of freedom make up the element. For the concrete model, solid pieces were employed with a 50-mm mesh size. The study’s concentrated load was applied at the top of a pair of transverse rollers and split into many loads at the top mesh joint in the y direction. In the concrete model, where there are two supports, two boundary conditions must be implemented (hinged and roller supports), as shown in Fig. 24.

SOLID 45: 3D load plate and supports: The solid 45 pieces are used as a model for the load plate and supports. Eight nodes make up the element, and each node has three degrees of freedom. Two transverse rollers were subjected to the concentrated load utilized in this investigation at their tops. At the top mesh junction, the force was divided into many loads in the y direction. In the concrete model, when there are two supports (hinged and roller supports), two boundary conditions must be implemented, as shown in Fig. 25.

Table 10 In contrast to the ultimate load results

Specimens	Ultimate load (kN)		% Diff
	Numerical	Experimental	
BH1	275.5	268.57	2.6
BH2	287.5	269.83	6.5
BRH1	245	237.19	3.3
BRH2	252.5	239.68	5.3
BRH3a	232.5	230.19	1.0
BRH4	245	234.41	4.5
BRH5	227.5	222.14	2.4
BRH6	230	226.67	1.5

Diff. = differential

Table 11 In contrast to the maximum mid-deflection results at the collapse

Specimens	Maximum central deflection (mm)		% Diff
	Numerical	Experimental	
BH1	45.2	50.42	- 10.4
BH2	50	51.3	- 2.5
BRH1	48.5	52.77	- 8.1
BRH2	51.52	57.67	- 10.7
BRH3a	47	55.1	- 14.7
BRH4	50	50.7	- 1.4
BRH5	49.31	54.42	- 9.4
BRH6	52.22	58.65	- 11.0

Diff. = differentia

7 Validation of Numerical Model

Validation was based on the experimental results with the analytical results using ANSYS. The numerical model with the application for finite element analysis (ANSYS 15) showed valuable results regarding the ultimate failure load, maximum central deflection, crack pattern and ductility.

7.1 Failure Load and Maximum Deflection at Mid-Span

The comparison of the greatest central deflection and ultimate loads is listed in Tables 10, 11. The results acquired by the numerical model were compared to the experimental results. A decrease in the ultimate failure load values of the numerical model by approximately 1% up to 6.5% compared to the experimentally acquired data was observed, and also decrease in the central deflection values by 1.4% up to 14.7% was obtained. The deflection results for all beams are listed in Table 11. It can be seen that all beams had linear behavior from

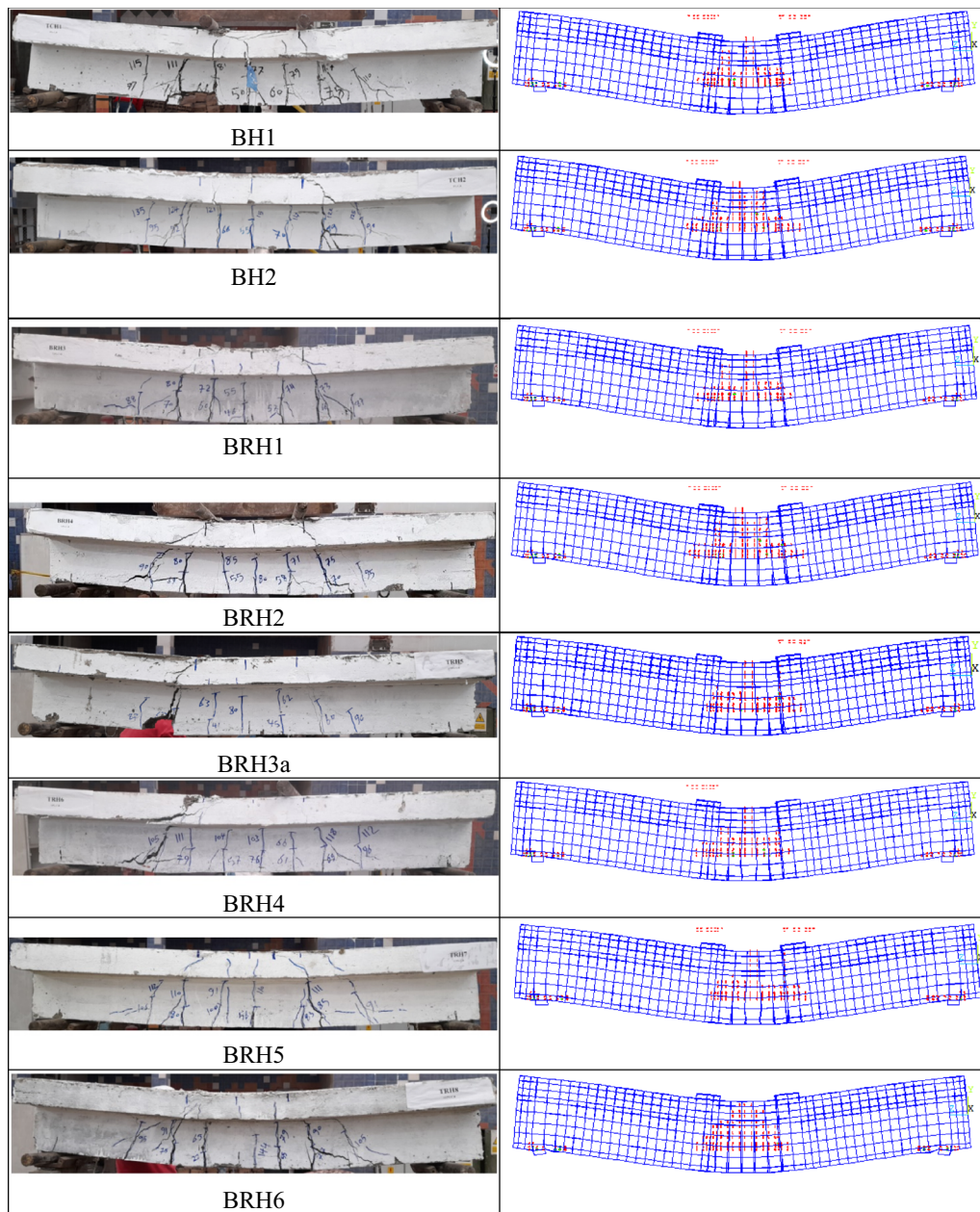


Fig.26 Numerical and experimental crack patterns for beams

initial loading up to the first crack, followed by a non-linear response after cracking.

7.2 Crack Patterns

Fig. 26 shows the crack pattern after failure, acquired by both the analytical and experimental results for all beams. The load was applied progressively until the failure of the beam. The final failure occurred near the

mid-span. The numerical results agree well with the experimental results recording the crack pattern.

The results demonstrate that increasing the diameter of GFRP bars significantly increases the ultimate capacity and deflection of RC beams. The hybrid reinforcement ratio is investigated as a critical parameter to improve the flexural performance of hybrid rubberized concrete HRC reinforced with GFRP bars, and steel bars (Qin et al., 2017). The experimental results were validated and compared to those obtained from

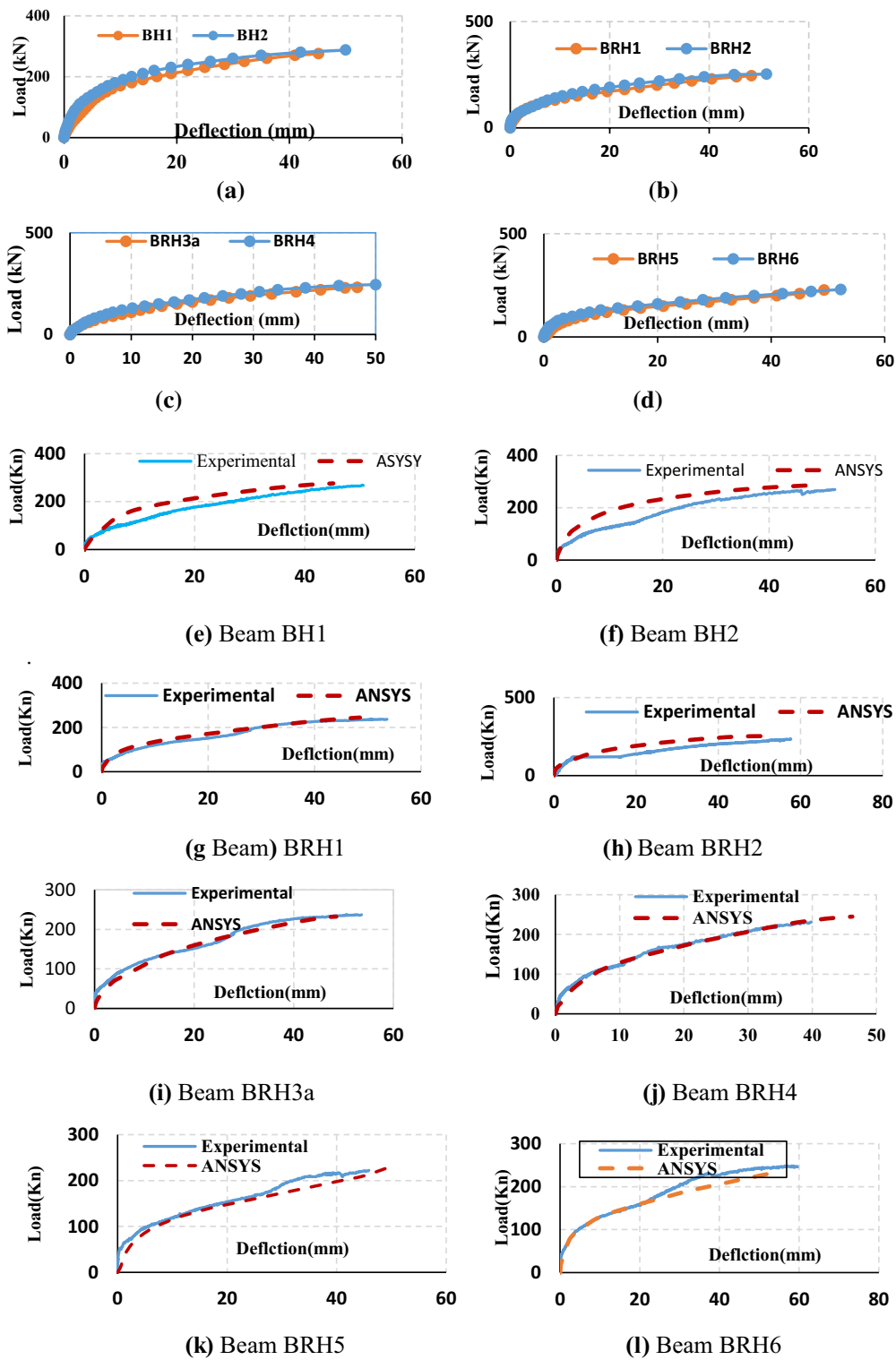


Fig. 27 Comparison of numerical and experimental results

ANSYS software-based non-linear finite element analysis shown in Fig. 27a, d. The numerical results obtained from (ANSYS 15) agree well with the experimental results in terms of crack pattern as well as the ultimate load. The mid-deflection obtained using ANSYS matched the outcomes of the experiment for a lower range of load values for all beams. For higher loads, there was a slight deviation between the experimental and finite element results, as shown in Fig. 26e, l.

7.3 In Contrast to the Experimental Results and the Numerical Results by ANSYS

The numerical results obtained from (ANSYS 15) correspond well with the experimental findings about the ultimate load and the crack pattern. The mid-deflection obtained using ANSYS matched the experimental results for a lower range of load values for all beams. For higher loads, there was a slight deviation between the experimental and finite element results, as shown in Fig. 26.

7.4 Ductility Index

The ductility index is calculated as:

Maximum deflection (85% of the peak load) / yield deflection equals the ductility index. The ductility index comparison is displayed in Table 12. The experiment's results and the numerical model's obtained results diverge. It was found that the numerical model's ductility factor values were lower by about 8.3% when compared to the one obtained experimentally. The numerical results and the experimental results correspond well. The results of the finite element model show that the necessary strength and ductility performance may be obtained by appropriately engineering the hybrid reinforcement ratio. (Qin et al., 2017). It is shown that the proposed formulations yield reliable estimates of the strength and ductility of reinforced rubberized concrete members, which

makes them suitable for use in both practical applications and codified norms (Xu et al., 2020).

8 Conclusion

Based on the experimental program's attained results, which were also contrasted with the results of non-linear finite element analysis performed with ANSYS software, the following conclusions were obtained:

1. The ultimate failure load for the tested hybrid rubberized T-beam BRH1, BRH3a and BRH5 (7.5%, 10%, and 12.5% C.R) decreased by 11.68%, 14.29%, and 17.47%, respectively, compared to the hybrid T-beam BH1(0% C.R). Also BRH2, BRH4 and BRH6 (7.5%, 10%, and 12.5% C.R) were lower than the hybrid beam BH2 (0% C.R) by 13%, 15.72%, and 15.99, respectively, indicating that the load capacity of hybrid rubberized-T RC beams decreased concerning hybrid T-beams with 0% C.R.
2. The mid-span maximum deflection for the tested hybrid rubberized T-beam BRH1, BRH3a and BRH5 (7.5%, 10%, and 12.5% C.R) increased by 4.66%, 9.28%, and 15%, respectively, compared to the hybrid T- beam BH1(0% C.R). Also for BRH2, BRH4 and BRH6 (7.5%, 10%, and 12.5% C.R) the mid-span deflection increased compared to BH2 (0% C.R) by 5.26%, 9.16%, and 14.32, respectively.
3. The ductility index for the tested rubberized hybrid T-beams BRH1, BRH3a and BRH5 were higher than BH1 by 28.2%, 35.47%, and 65.38%, respectively, indicating that increasing the percentage of C.R has a direct effect on increasing the ductility index. Also BRH2, BRH4, and BRH6 were higher than BH2 by 23.76%, 30.04%, and 56.95%, respectively, indicating that the ductility index of hybrid-rubberized RC T-beams with (7.5%, 10%, and 12.5% C.R) increased compared to hybrid normal R.C T-beams (0% C.R).
4. It was noted that increasing the diameter of GFRP bars from 10 to 12 mm resulted in a decrease in the ductility index (7.5%, 10%, and 12.5%). Increasing the diameter of GFRP bars from 10mm in BH1 to 12 mm in BH2 resulted in a decrease in the ductility index by 4.7% yet the existence of C.R in BRH1 compared to BH1 resulted in regaining an increase in the ductility index by 28%.
5. The energy dissipation decreased for hybrid-rubberized T-beams BRH1, BRH3a and BRH5 (7.5%, 10%, and 12.5% C.R) by 7.88%, 12.36%, and 17.17%, respectively, compared to T-beam BH1 (0% C.R). This indicates that the existence of the very weak crumb rubber was not able to dissipate the energy properly within the concrete matrix, which is an indication of a slight lack of compatibility. Also the BRH2, BRH4

Table 12 In contrast to the ductility factor results

Specimens	Ductility factor		% Diff
	Numerical	Experimental	
BH1	2.19	2.34	- 6.4
BH2	2.15	2.23	- 3.6
BRH1	2.81	3	- 6.3
BRH2	2.58	2.76	- 6.5
BRH3a	2.96	3.17	- 6.6
BRH4	2.73	2.9	- 5.9
BRH5	3.65	3.87	- 5.7
BRH6	3.21	3.5	- 8.3

Diff. = differential

and BRH6 with (7.5%, 10%, and 12.5% C.R) by 8.12%, 12.96%, and 18.28% times, respectively, compared to RC T-beam BH2 (0% C.R).

- Regarding the final failure loads and the fracture pattern, the finite element calculations and the experimental data are in agreement. A decrease in the ultimate failure load values for the numerical model by approximately 1% up to 6.5% compared to the experimentally acquired data was observed.

Abbreviations

FRC	Fiber-reinforced concrete
FRP	Fiber-reinforced polymer
GFRP	Glass fiber-reinforced polymer
HGFRP	Hybrid glass fiber-reinforced polymer
C.R.	Crumb rubber
RC	Reinforced concrete
As	The area of steel bars
NC	Normal aggregate concrete
RRC	Rubberized recycled concrete
HRRC	Hybrid rubberized reinforced concrete
HRTB	Hybrid rubberized T-beam
fu	Ultimate tensile stress
Pcr	Flexural cracking load
Pu	Ultimate load
Cw	Width of crack
Nc	Number of crack
W	Weight
V	Volume
SP	Super-plasticizer
LVDTS	Linear variable differential transducers
Mu	Ultimate flexure of the cross sec.
HRTB	Hybrid rubberized T-beam
Ed	Energy dissipation

Acknowledgements

Not applicable.

Author contributions

TS: numerical modeling and final draft editing, AG: design the experimental program methodology and final review. MS: performed the experimental program and original draft. All authors read and approved the final manuscript.

Funding

Open access funding provided by The Science, Technology & Innovation Funding Authority (STDF) in cooperation with The Egyptian Knowledge Bank (EKB).

Availability of data and materials

All data generated or analyzed during this study are included in this published article.

Declarations

Ethics approval and consent to participate

Not applicable.

Consent for publication

Not applicable.

Competing interests

There is no competing interest associated with the submission of this manuscript.

Received: 23 September 2023 Accepted: 17 February 2024

Published online: 21 May 2024

References

- AbdelAleem, B. H., Ismail, M. K., & Hassan, A. A. (2018). The combined effect of crumb rubber and synthetic fibers on the impact resistance of self-consolidating concrete. *Construction and Building Materials*, *162*, 816–829.
- Ahmed Tareq Noaman. Effect crumb rubber aggregate on toughness and impact energy of steel fiber concrete, Ph.D. thesis, (January 2017). School of Civil Engineering University Sains Malaysia.
- Alam, I., Mahmood, U. A., & Khattak, N. (2015). Use of rubber as aggregate in concrete: a review. *International Journal of Advanced Structures and Geotechnical Engineering*, *4*(2), 92.
- Alasmari, H. A., Abu Bakar, B. H., & Noaman, A. T. (2019). A Comparative Study on the Flexural Behaviour of Rubberized and Hybrid Rubberized Reinforced Concrete Beams. *Civil Engineering Journal*, *5*(5), 1052.
- Al-Tayeb, Mustafa Maher, B. H. Bakar, Hanafi Ismail, and Hazizan Md Akil. Experimental and Nonlinear Dynamic Analysis of Hybrid Powder Rubberized-Normal Concrete under Impact Load. *Caspian Journal of Applied Sciences Research* 1, no. 11 (2012).
- Ashour, A. F. (2006). Flexural and shear capacities of concrete beams reinforced with GFRP bars. *Construction and Building Materials*, *20*, 1005–1015.
- ASTM International, ASTM C 494/C494M-19e1, Standard Specification for Chemical Admixtures for Concrete, (2020).
- Atahan, A. O., & Yücel, A. Ö. (2012). Crumb rubber in concrete: Static and dynamic evaluation. *Construction and Building Materials*, *36*, 617–622.
- Atahan, A. O., & Yucel, A. O. (2013). Resources, Laboratory and field evaluation of recycled content sign posts. *Conservation and Recycling*, *73*, 114–121.
- Benmokrane, B., Chaallal, O., & Masmoudi, R. (2021). Flexural response of concrete beams reinforced with FRP reinforcing bars. *Case Studies in Construction Materials*, *14*, e00513–e516.
- Bischoff, P. H. (2007). Deflection calculation of FRP reinforced concrete beams based on modifications to the existing Branson equation. *Journal of Composites for Construction*, *11*, 4–14.
- Eisa, A. S., Elshazli, M. T., & Nawar, M. T. (2020). Experimental investigation on the effect of using crumb rubber and steel fibers on the structural behavior of reinforced concrete beams. *Construction and Building Materials*. <https://doi.org/10.1016/j.conbuildmat.2020.119078>
- Erfan, A. M., AbdElnaby, R. M., Badr, A., & El-sayed, T. A. (2021). Flexural behavior of HSC one way slabs reinforced with basalt FRP bars. *Case Studies in Construction Materials*, *14*, e00513.
- Guo, Y. C., Zhang, J. H., Chen, G., Chen, G. M., & Xie, Z. H. (2014). "Fracture behaviors of a new steel fiber reinforced recycled aggregate concrete with crumb rubber. *Construction and Building Materials*, *53*, 32–39.
- Guo, Y. C., Zhang, J. H., Chen, G., Chen, G. M., & Xie, Z. H. (2014). Fracture behaviors of new steel fiber reinforced recycled aggregate concrete with crumb rubber. *Construction and Building Materials*, *53*, 32–39.
- Ismail, M. K., & Hassan, A. A. A. (2017). An experimental study on flexural behavior of large-scale concrete beams incorporating crumb rubber and steel fibers. *Engineering Structures*, *145*, 97–108.
- Kaewunruen, S., Li, D., Chen, Y., & Xiang, Z. (2018). Enhancement of dynamic damping in eco-friendly railway concrete sleepers using waste-tyre crumb rubber. *Materials*, *11*(7), 1169.
- Kara, I. F., & Ashour, A. F. (2012). Flexure design methodology for concrete beams reinforced with fiber-reinforced polymers. *Composite Structures*, *94*, 1616–1625.
- Liu, F., Chen, G., Li, L., & Guo, Y. (2012). Study of the impact performance of rubber reinforced concrete. *Construction and Building Materials*, *36*, 604–616.
- Mendis, A. S. M., Al-Deen, S., & Ashraf, M. (2018). Flexural shear behavior of reinforced crumbed rubber concrete beam. *Construction and Building Materials*, *166*, 779–791.
- Miraldo, S., Lopes, S., Torgal, F. P., & Lopes, A. (2021). Advantages and shortcomings of the utilization of recycled wastes as aggregates in structural concretes. *Construction and Building Materials*. *V*, *298*, 123729.

- Moolaei, S., Sharbatdar, M. K., & Kheyroddin, A. (2021). Experimental evaluation of flexural behavior of HPFRCC beams reinforced with hybrid steel and GFRP bars. *Composite Structures*, 275, 114503.
- Najim, K. B., & Hall, M. R. (2010). A review of the fresh/hardened properties and applications for plain- (PRC) and self-compacting rubberised concrete (SCRC). *Construction and Building Materials*, 24(11), 2043–2051.
- Najim, K. B., & Hall, M. R. (2012). Mechanical and dynamic properties of self-compacting crumb rubber modified concrete. *Construction and Building Materials*, 27(1), 521–530.
- Oikonomou, N., & Mavridou, S. (2009). The use of waste tyre rubber in civil engineering works. *Sustainability of Construction Materials*. <https://doi.org/10.1533/9781845695842.213>
- Onuaguluchi, O., & Panesar, D. K. (2014). Hardened properties of concrete mixtures containing pre-coated crumb rubber and silica fume. *Journal of Cleaner Production*, 82, 125–131.
- Ozbay, E., Lachemi, M., & Sevim, U. K. (2010). Compressive strength, abrasion resistance and energy absorption capacity of rubberized concretes with and without slag. *Materials and Structures*, 44(7), 1297–1307.
- Qin, R., Zhou, Ao., & Lau, D. (2017). Effect of reinforcement ratio on the flexural performance of hybrid FRP reinforced concrete beams. *Composites Part B: Engineering*, 108(1), 200–209.
- Rasheed, H. A., Naye, I. R., & Melhem, H. (2004). Response prediction of concrete beams reinforced with FRP bars. *Composite Structures*, 65, 193–204.
- Razaqpur, A. G., Svecova, D., & Cheung, M. S. (2000). Rational method for calculating deflection of fiber reinforced polymer reinforced beams. *ACI Structural Journal*, 97, 175–184.
- Said, M., Mustafa, T. S., Shanour, A. S., & Khalil, M. M. (2020). Experimental and analytical investigation of high-performance concrete beams reinforced with hybrid bars and polyvinyl alcohol fibers. *Construction and Building Materials*, 259, 120395.
- SAS IP. (1999). *ANSYS theory reference release 15*. ANSYS, Inc.
- Sukontasukkul, P., Jamnam, S., Rodsin, K., & Banthia, N. (2013). Use of rubberized concrete as a cushion layer in bulletproof fiber reinforced concrete panels. *Construction and Building Materials*, 41, 801–811.
- Sun, Z., Fua, L., Feng, D., Vatuloka, A. R., Wei, Y., & Wu, G. (2019). Experimental study on the flexural behavior of concrete beams reinforced with bundled hybrid steel/FRP bars. *Engineering Structures*, 197, 109443.
- Thomas, B. S., Gupta, R. C., Mehra, P., & Kumar, S. (2015). Performance of high strength rubberized concrete in an aggressive environment. *Construction and Building Materials*, 83, 320–326.
- Toutanji, H., & Deng, Y. (2003). Deflection and crack-width prediction of concrete beams reinforced with glass FRP rods. *Construction and Building Materials*, 17, 69–74.
- Toutanji, H., & Saafi, M. (2000). Flexure behavior of concrete beams reinforced with glass fiber-reinforced polymer (GFRP) bars. *ACI Structural Journal*, 97, 712–719.
- Vijay, P. V., & Gangarao, H. V. V. (2001). bending behavior and deformability of glass fiber reinforced polymer reinforced concrete members. *ACI Structural Journal*, 98, 834–842.
- Xie, J.-h., Guo, Y.-c., Liu, L.-s., & Xie, Z.-h. (2015). Compressive and flexural behaviors of a new steel-fiber-reinforced recycled aggregate concrete with crumb rubber. *Construction and Building Materials*, 79, 263–272.
- Xu, B., Bompa, D. V., Elghazouli, A. Y., Ruiz-Teran, A. M., & Stafford, P. J. (2020). Numerical assessment of reinforced concrete members incorporating recycled rubber materials. *Engineering Structures*, 204, 110017.
- Yost, J. R., & Gross, S. P. (2002). Flexure design methodology for concrete beams reinforced with fiber-reinforced polymers. *ACI Structural Journal*, 99, 308–316.
- Zheng, L., Sharon Huo, X., & Yuan, Y. (2008). Experimental investigation on dynamic properties of rubberized concrete. *Construction and Building Materials*, 22(5), 939–947.

Amr A. Gamal Professor, Structural Engineering Department, Shoubra Faculty of Engineering, Benha University, EGYPT.

Mohamed Essam Sayed PhD Candidate, Structural Engineering Department, Shoubra Faculty of Engineering, Benha University, EGYPT.

Publisher's Note

Springer Nature remains neutral with regard to jurisdictional claims in published maps and institutional affiliations.

Tarik S. El-Salakawy Associate Professor, Structural Engineering Department, Shoubra Faculty of Engineering, Benha University, EGYPT.